Experimental Evidence of Primary Permeability at Very Low Gas Content in Crystal-Rich Silicic Magma

Anna Theurel, Marielle Collombet, Alain Burgisser, Caroline Martel, Caroline Martel, Laurent Arbaret, Rémi Champallier

AGU ADVANCING EARTH AND SPACE SCIENCES

Geophysical Research Letters

RESEARCH LETTER
10.1029/2024GL108389

Experimental Evidence of Primary Permeability at Very Low Gas Content in Crystal-Rich Silicic Magma

Anna Theurel[1], Marielle Collombet[1], Alain Burgisser[1], Caroline Martel[2], Laurent Arbaret[2], and Rémi Champallier[2]

[1]University Grenoble Alpes, University Savoie Mont Blanc, CNRS, IRD, IFSTTAR, ISTerre, Grenoble, France, [2]Institut des Sciences de la Terre d'Orléans (ISTO), University Orléans, CNRS, BRGM, Orléans, France

Key Points:

- Gas permeability in silicic magma is possible with gas volumes below 10% thanks to high crystallinity
- Outgassing at low gas content can happen without external deformation nor fracturation of the magma
- Volcanic outgassing in stagnant magmas is explained by deep conduit bubble channeling that may be a key mechanism in eruptive transition

Supporting Information:

Supporting Information may be found in the online version of this article.

Correspondence to:

A. Theurel,
anna.theurel@univ-smb.fr

Citation:

Theurel, A., Collombet, M., Burgisser, A., Martel, C., Arbaret, L., & Champallier, R. (2024). Experimental evidence of primary permeability at very low gas content in crystal-rich silicic magma. *Geophysical Research Letters*, *51*, e2024GL108389. https://doi.org/10.1029/2024GL108389

Received 23 JAN 2024
Accepted 7 MAY 2024

Author Contributions:

Conceptualization: Anna Theurel, Marielle Collombet, Alain Burgisser, Caroline Martel
Data curation: Anna Theurel
Formal analysis: Anna Theurel
Funding acquisition: Marielle Collombet, Alain Burgisser, Laurent Arbaret
Investigation: Anna Theurel, Marielle Collombet, Alain Burgisser, Caroline Martel
Methodology: Anna Theurel, Caroline Martel, Laurent Arbaret, Rémi Champallier
Project administration: Marielle Collombet, Alain Burgisser, Caroline Martel
Resources: Marielle Collombet, Alain Burgisser, Caroline Martel, Laurent Arbaret, Rémi Champallier

Abstract Eruptive dynamics is influenced by gas escape from the ascending magma. Gas pathways form in the magma via bubble coalescence, leading to gas channeling. Magmatic crystals play a key role in gas channel formation. This work constrains experimentally decompression-induced coalescence in high-crystallinity silicic magmas without external deformation, focusing on low gas content and bimodal crystal size (microlites and phenocrysts). All percolating samples have permeabilities of 10^{-14} m^2 at bulk porosities of 7–10 vol% and bulk crystallinities up to 75 vol%. Our results demonstrate the possibility of coalescence-related outgassing at high pressure (120–350 MPa) and without external strain, which corresponds to magma stagnating deep in a volcanic conduit. Channeling at such low gas content implies that bimodal crystallinity favors effusive over explosive volcanic behavior. It may also be the missing physical mechanism explaining gas transfer across magmatic systems despite high melt viscosity and low or absent magma extrusion.

Plain Language Summary The way volcanoes erupt is mainly controlled by the ability of gases to escape from the magma (outgassing). An efficient way to outgas is to connect bubbles together (coalescence) up to the point where channels form in the magma (channeling) in which gas can circulate toward the surface. We investigate experimentally how coalescence and channeling happen in immobile, crystal-rich viscous magma in conditions (pressure and temperature) similar to those found in deep volcanic conduit, where only a small amount of gas (<10%) is present. Our experiments demonstrate that bubble connections are possible thanks to a large amount of crystals on which bubbles can lean, deform, and join each other. That gas can escape from magma at depth could favor effusive eruption over volcanic explosions and even bring new insights on degassing in immobile magma.

1. Introduction

Magma outgassing plays a crucial role in eruptive dynamics. When the gas phase remains in the conduit, conditions propitious to fragmentation can be met, leading to explosive behavior (Gonnermann & Manga, 2007). If the permeability is sufficiently high within the magma, outgassing can evacuate enough gas from the ascending magma to remain below the fragmentation threshold. In the case of silica-rich magmas often involved in eruptions prone to behave effusively and explosively during a single eruptive episode, the melt is so viscous (>10^4 Pa.s) (Hess & Dingwell, 1996) that gas bubbles cannot ascend within the conduit by buoyancy alone (Lindoo et al., 2017), calling for alternate outgassing mechanisms. Many active volcanoes show near-constant outgassing at the vent, even without magma extrusion (Christopher et al., 2015; Edmonds et al., 2010). This implies outgassing without magma ascent into the conduit and without magma deformation along the conduit margins. In addition, many crystal-rich samples coming from deep conduit zones (~5–10 km) and ejected during Vulcanian eruption present gas content substantially lower than theoretically predicted by closed system degassing (Collombet et al., 2021; Drignon et al., 2016), suggesting that a non-negligible amount of gas has already been extracted before eruption despite being at great depth.

Several processes can lead to outgassing. At low gas volume fraction (<10 vol% bulk), the gathering and coalescence of several bubbles alongside can lead to the development of narrow gas pathways that enable the gas to extract itself efficiently from the magmatic column. We refer to this process as channeling to distinguish it from the highly interconnected bubble networks forming at high gas volume fraction (>30 vol%, Giachetti et al., 2019). Crystals serve as a framework that fosters the peculiar form of bubble coalescence characteristic of channeling (Burgisser et al., 2020; Cáceres et al., 2022; deGraffenried et al., 2019; Parmigiani et al., 2017) by reducing the space in the melt where bubbles can nucleate and grow, thus promoting proximity.

Software: Anna Theurel, Marielle Collombet, Alain Burgisser, Laurent Arbaret
Supervision: Marielle Collombet, Alain Burgisser, Caroline Martel
Validation: Marielle Collombet, Alain Burgisser
Visualization: Anna Theurel, Alain Burgisser, Laurent Arbaret
Writing – original draft: Anna Theurel
Writing – review & editing: Marielle Collombet, Alain Burgisser, Caroline Martel, Laurent Arbaret

Numerical and empirical models have given rise to different hypotheses on the role of crystals in gas channel formation; crystals sizes, volume fraction, shape and orientation are all likely to control coalescence (Bretagne et al., 2023; Collombet et al., 2021; Degruyter et al., 2019; Klug & Cashman, 1996; Mueller et al., 2005; Parmigiani et al., 2017; Vasseur et al., 2022; Wadsworth et al., 2021). It is yet unclear which of these geometrical factors are key in promoting gas percolation at very low gas content in the absence of strain. In this study, we performed decompression experiments in an internally-heated pressure vessel to investigate the influence of crystal content and sizes on channeling development in synthetic magmas and, thus, on permeability in immobile, gas-poor magmas. We evidence percolation by channeling at low gas content and high pressure that implies a new mechanism of deep outgassing for stagnant magmas.

2. Materials and Methods

2.1. Materials

Our three-phase magmas contain liquid (melt), gas (bubbles), and solid (crystals). The melt was made of an anhydrous powder of haplotonalite glass (HTN in wt%: 69.0 SiO_2, 19.9 Al_2O_3, 3.5 CaO, and 7.6 Na_2O), which is a good proxy for a high viscosity rhyolitic melt (Mollard et al., 2012). Distilled pure water was used to model the gas phase. Enough water was added to the HTN glass at initial pressure (350 MPa) to exsolve about 10 vol% bulk of water bubbles at final pressure (120 MPa) following Jaupart & Allègre, 1991. The solid phase was composed of a mixture of three crystal sizes commonly observed in natural volcanic samples: phenocrysts (hundreds of μm) mostly growing in magma chambers, microphenocrysts (∼50–100 μm) and microlites (<50 μm) crystallizing under low and high undercooling, respectively, during magma ascent toward the surface. The phenocryst and microphenocryst populations were represented by equant alumina crystals (insulating powder from Friatec AG, Germany) manually sieved to ∼300 and ∼50 μm, respectively. These two populations of alumina crystals were added to the HTN glass to reach targeted proportions from 0 to 50 vol%. The microlite population was represented by plagioclases directly growing from the water-saturated HTN melt during hydration at initial pressure and temperature. Of the eight starting materials, two contain only plagioclase microlites, two contain plagioclase microlites plus alumina microphenocrysts, two contain plagioclase microlites plus alumina phenocrysts, and two contain plagioclase microlites plus both sizes of alumina crystals (Table 1).

2.2. Experimental Procedure

Gold capsules of 15 mm in length and 5.4 mm in inner diameter were filled with about 50 mg HTN powder, the alumina crystals when relevant, and water. Each capsule was subjected to mass balance and leakage tests to guarantee that it was hermetically sealed. The eight capsules were oriented vertically and loaded in a Kh furnace that was inserted in a vertical pressure vessel (Martel, 2012). The pressure medium was pure argon and pressure was measured using a transducer calibrated against a Heise Bourdon gauge (accuracy of ±0.2 MPa). The temperature was continuously measured by K-type thermocouples (precision of ±3°C). The autoclave was heated at 850°C and pressurized to 350 MPa and maintained at these conditions for at least 18 hours (overnight) to ensure water diffusion in the melt and plagioclase crystallization. After this hydration and crystallization step, we performed an isothermal decompression from 350 to 120 MPa at 1.3 MPa/s (about 4 min) to cause bubble growth. The result of this decompression is described in Figure S4 in Supporting Information S1. Samples were then held at 120 MPa and 850°C during 1 h 30 min before being rapidly cooled down to room temperature at a rate of 2°C/s. At 250°C, well below the solidus, the autoclave was decompressed to ambient pressure, and the capsules were extracted, weighed to test for possible leakage, and opened carefully to recover the sample as one piece.

2.3. Analytical Methods

To image the samples, we used a Phoenix Nanotom 180 X-ray computed microtomograph (μCT; ISTO) with a molybdenum target, a tungsten filament, a variable operating voltage of 68–94 kV and a filament current of 50–210 nA. Samples were rotated over 360° during the exposure to the X-radiation. The 3D volumes were reconstructed using in-house Phoenix software. The average resolution (voxel edge length) of the volumes is 3 μm. This resolution is insufficient to image plagioclase microlites (Figure 1a) accurately. Moreover, as the density of plagioclase is very similar to that of glass, the two phases share the same range of attenuation intensity (voxel greyscale value) and are, therefore, indistinguishable. To overcome this, we also imaged polished sections of all samples by Scanning Electron Microscopy (SEM) with a JEOL JSM-6400 microscope operating at 15–20 kV

Table 1
Sample Description

	Crystals[a]				Gas bubble[b]				Melt[c]
Run	Crystal size (μm)	Φ_{Al} vol%	Φ_{Plag} vol%	$\Phi_{Al + Plag}$ vol%	Φ_{Gas} vol%	Φ_{Gas}c vol%	logBND	logK[d]	Φ_{Melt} vol%
1	**10 + 50**	**50.1**	**21.2**	**71.3**	**9.8**	**7.1**	**11.6**	**−13.9**	**18.9**
2	**10 + 300**	**44.8**	**25.4**	**70.2**	**7.1**	**7.4**	**10.4**	**−14.0**	**22.7**
3	**10 + 50+300**	**37.9**	**28.4**	**66.3**	**8.5**	**8.3**	**11.3**	**−13.8**	**25.2**
4	10	–	45.3	45.3	14.5	13.6	11.3	No	40.2
5	**10 + 50**	**48.7**	**22.0**	**70.7**	**9.7**	**7.2**	**11.6**	**−13.9**	**19.6**
6	10 + 300	41.1	27.7	68.8	6.5	7.7	10.3	No	24.7
7	10 + 50+300	50.6	22.7	73.4	6.4	6.6	10.4	No	20.2
8	10	–	45.0	45.0	15.0	13.6	11.5	No	40.0

Note. Bold lines correspond to permeable sample. [a]Crystals consist of plagioclase microlites (Plag) of ∼10 μm, alumina microphenocrysts and phenocrysts (Al) of ∼50 and 300 μm, respectively. Contents of Plag (Φ_{Plag}) and Al (Φ_{Al}) are calculated on a bulk (bubble-bearing) basis. $\Phi_{Plag + Al}$ combines Φ_{Plag} and Φ_{Al}. [b]Predicted melt bubble content (Φ_{gas}c) is first calculated at 850°C after the equation of Jaupart and Allègre (1991) with the water content introduced in the capsule as initial water content and 120 MPa as final pressure, and then recalculated on a bulk (crystal-bearing) basis. The bulk bubble content (Φ_{gas}) and bubble number density (BND) recalculated on a melt basis are determined from μCT analyses. The permeability (K) is determined from the μCT images using the Palabos software. [c]The bulk melt content (Φ_{melt}) is 100-$\Phi_{Plag + Al}$-Φ_{gas}. [d]Label "No" means that no continuous voxel chain connects two opposite ends of the sample, that is, there is no percolation.

acceleration voltages (ISTO). The resolution (pixel edge length) of our SEM images (Figures 1c and 1d) ranges from 1.5 to 0.01 μm. SEM images were primarily used to constrain plagioclase microlites size, shape, number density, and orientation. They allowed us to ensure the homogeneity of the microlite crystallization across the series, thus enabling robust comparisons between samples.

All additional analyses were performed on the μCT and SEM images acquired using FiJi/ImageJ software phase segmentation. We used the Palabos model to check face-to-face percolation of the volumes (Figure 1b) and calculate the permeability of the gas phase in all three directions by solving the Lattice-Boltzman equations as detailed in Burgisser et al. (2017).

3. Results

3.1. Sample Textures

After decompression from 350 to 120 MPa, all samples were three-phased (crystals, melt, gas) in proportions and properties reported in Table 1. SEM observations of the plagioclase microlites show a monodisperse crystal size distribution between 5 and 20 μm for long axes (Figure S1 in Supporting Information S1, Morgan & Jerram, 2006) and up to 3 μm for the short axis (hereafter referred to as 10 μm microlites). Plagioclase proportion is systematically 53 ± 3 vol% with respect to the melt. Visual inspection of the volumes suggests that alumina crystals are homogeneously distributed throughout the samples. Microlites are particularly present along alumina crystals that act as preferential nucleation sites for plagioclase. In alumina-free samples, microlites are distributed homogeneously in the melt. The SEM images (Figures 1c and 1d) also reveal that plagioclase crystals surround nearly all the bubbles; very few bubbles are in direct contact with alumina crystals. Some alumina crystals are fractured but not displaced. We attribute these cracks to contact points between larger crystals during the high pressure synthesis (Forien et al., 2011). These cracks are only visible on the SEM images due to their minimal thickness. They do not participate in the permeable network as no crack is longer than the typical crystal size.

There are four bubble populations based on their texture and sizes, ranging from an isolated, 1–4 μm population to a 5–8 μm population displaying incipient coalescence that transitions into a 8–100 μm population featuring coalesced bubbles. The last population is composed of a few bubble chains that cause percolation when spanning the sample length (Figure S2 in Supporting Information S1). Isolated bubbles and bubble chains are homogeneously distributed within the melt-microlite mixture.

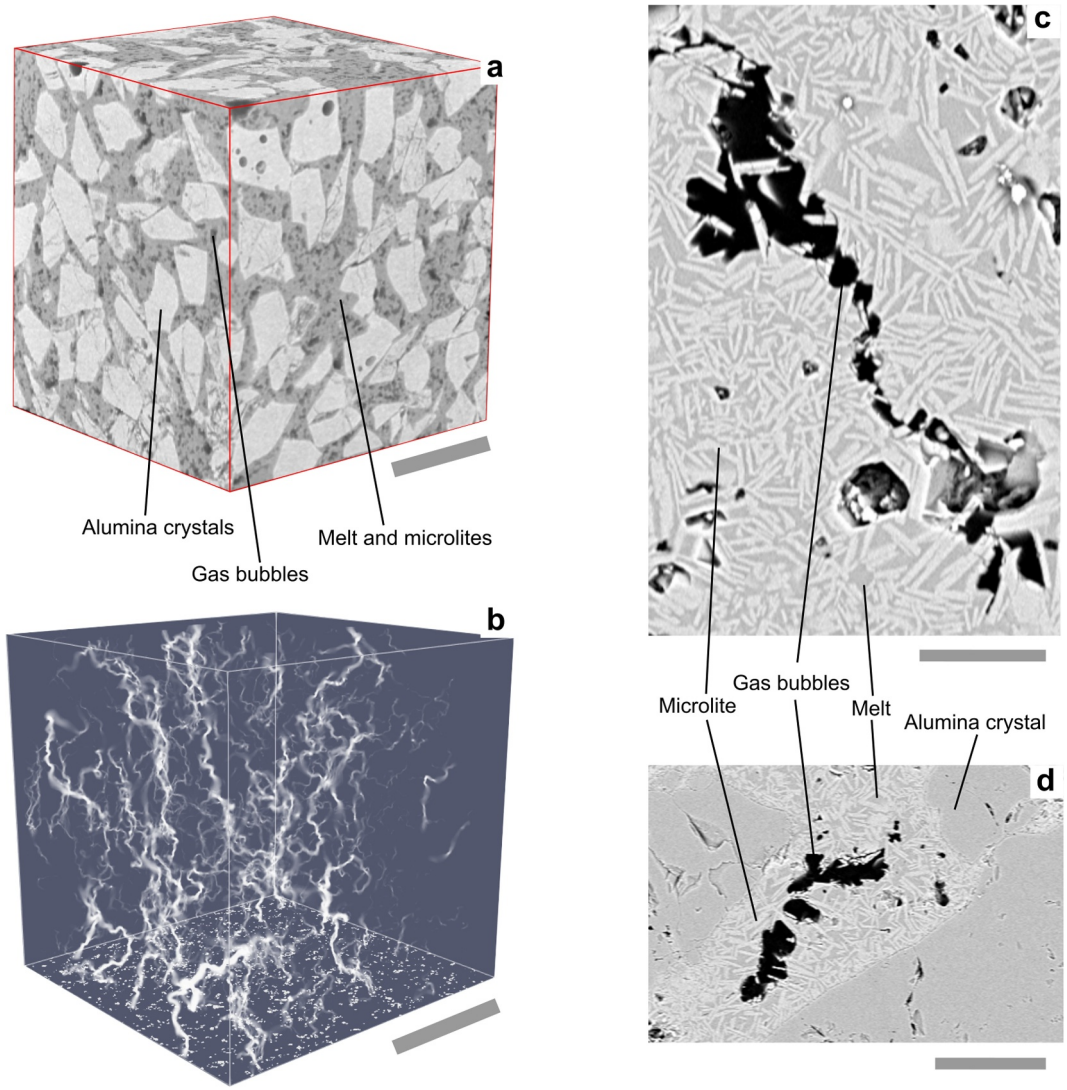

Figure 1. Vizualisation of the samples. (a) Reconstructed volume of a sample via μ-tomographic images (run 1, scale bar is 200 μm) (b) Rendering of gas flow (white gradient is velocity magnitude) in a permeable sample obtained from numerical simulation (run 1, scale bar is 200 μm) (c) Scanning Electron Microscopy (SEM) image showing percolating bubble chain when coalescence just happened (run 6, scale bar is 20 μm) (d) SEM image showing multiple bubble clusters (already resulting from coalescence) close to coalesce with each other (run 7, scale bar is 50 μm).

3.2. Permeability Occurrence

Among the eight samples, four are permeable with mean values of 10^{-14} m^2 (Table 1). Samples are permeable in one or two directions with no preferential orientation of the permeability nor significant trend in the direction of gravity. Permeability is isotropic and it ranges from 1×10^{-14} to 1.55×10^{-14} m^2. All permeable samples have less than 10 vol% bulk gas, which corresponds to a melt vesicularity of 24–34 vol%. None of the samples without alumina crystals is permeable and neither are the samples with less than 7 vol% bulk gas. This permeability is made possible by the coalescence of juxtaposed bubbles which form long chains across the samples (Figure 1b). We therefore demonstrate experimentally that channeling leads to possible gas percolation through the medium.

Our experiments were conducted in a non-deforming environment. It is known that shear deformation of magma leads to strong deformation of the bubbles, possibly enhancing coalescence (Burgisser & Gardner, 2004; Caricchi et al., 2011; Daffos et al., 2024; Laumonier et al., 2011; Lavallée et al., 2022). This deformation elongates bubbles in the shear direction, which reduce surface tension forces along their long edges. Low surface tension forces facilitate coalescence at the expense of areas of the bubble where higher forces dominate (i.e., where the curvature

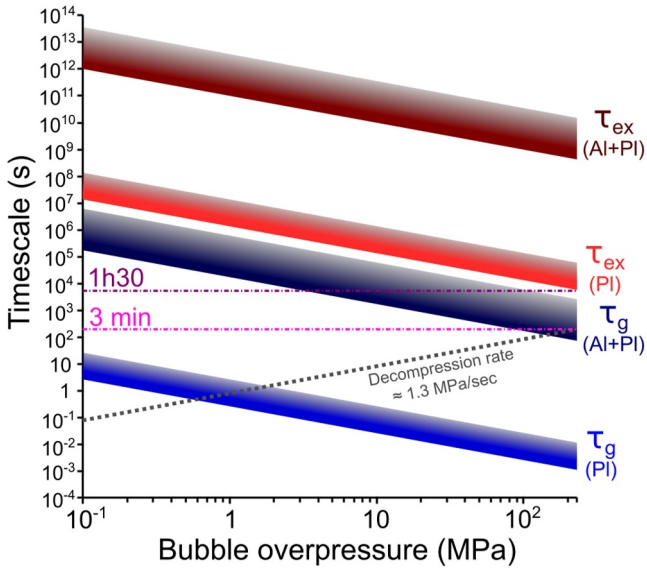

Figure 2. Theoretical estimates of the timescales of gas extraction (τ_{ex}) and bubble growth by viscous relaxation (τ_g) in crystal-rich magma as a function of bubble overpressure.

is greatest). Shear deformation of magma can therefore cause channeling (Daffos et al., 2024; Okumura et al., 2008, 2009) and hence fosters permeability. Our results imply that coalescence and subsequent channeling can take place at low porosity (albeit higher than 7 vol% bulk) and without shear deformation.

4. Discussion

4.1. Role of Crystals in Controlling Percolation

As explained below, the channeling we observe cannot easily be related to previous findings despite being in similar ranges of crystal and gas proportions. One reason is that gas escape cannot be captured by a single measure, such as permeability, connectivity, or percolation because it is a dynamic process. Connectivity (ratio of connected gas volume over total gas volume), for instance, is only loosely linked to percolation and permeability because clusters of coalesced bubbles may still be isolated from one another (Giachetti et al., 2019). Permeability can occur at low connectivity (0.06–0.54 in Graham et al., 2023; 0.1–0.3 in this study), whereas high connectivity does not imply percolation (Okumura et al., 2012).

Previous decompression experiments carried out with 20–50 vol% phenocrysts in the 50–355 μm size range yield contrasting results. Some studies concluded that crystal fraction, size, and shape play a modest control on gas percolation, making the critical melt vesicularity vary from 48 to 55 vol% (deGraffenried et al., 2019; Graham et al., 2023), which is well above the 24–34 vol% range we observe. Another study found no percolation up to 60 vol% melt vesicularity (Okumura et al., 2019) and a series of numerical studies extending the crystal content range to 40–75 vol% with 3–5 mm phenocrysts concluded that much lower percolation thresholds could be achieved (10 vol% melt vesicularity; Degruyter et al., 2019; Parmigiani et al., 2017). All the explanations proposed to resolve these apparent discrepancies put forward that high crystal contents foster multiple phenomena resulting in bubble coalescence. Crystals reduce the space in which bubbles can nucleate (deGraffenried et al., 2019; Graham et al., 2023) and, as they grow through viscous relaxation and/or exsolution, most find themselves constrained by the surrounding crystals, which force them to change from the spherical shape acquired at nucleation to a distorted shape with high local curvature (Degruyter et al., 2019; Parmigiani et al., 2017).

4.2. Surface Tension-Driven Process

The coalescence leading to the channeling described by Parmigiani et al. (2017) and Degruyter et al. (2019) was caused by viscous fingering due to high viscosity contrast of the phases and it was driven either by buoyancy or injection. These studies quantified the role of buoyancy by the Bond number (Bo = 0.1–1), which is the ratio of gravity forces over surface tension. In our samples, Bo ranges between 4×10^{-6} and 4×10^{-4} (with a melt-gas surface tension of 0.07 N/m) because of the small size of the bubbles (Figure S1 in Supporting Information S1). Surface tension forces thus dominate gravity forces by far in driving the coalescence we observe.

Another mechanism occurring during slow decompression of crystal-rich rhyolitic melts is gas segregation, which leads to porosity heterogeneities (Kobayashi et al., 2023; Okumura et al., 2019). We calculated (Figure 2) the timescales of gas extraction (τ_{ex}) and bubble growth by viscous relaxation (τ_g) in our experiments as, respectively, $\tau_{ex} = \frac{l^2 \varphi_g \eta}{k_X \Delta P}$ and $\tau_g = \frac{\eta}{\Delta P}$, where l is the length scale, φ_g is the volume fraction of the interstitial fluid phase, k_X is the permeability of the solid network, ΔP is the pressure difference between the bubble and the medium, and η is the strain-dependent magma viscosity (product of liquid viscosity and relative viscosity, Caricchi et al., 2007). Following Okumura et al. (2019), τ_{ex} corresponds to the duration of migration of the gas-melt mixture by permeable flow through the crystalline matrix due to a sample-wide pressure gradient caused by differential bubble growth. The resulting long durations suggest that gas segregation is not operating in our experiments because our crystal population yields too low a solid network permeability.

Bubble growth by viscous relaxation, τ_g, is controlled by the ratio of magma viscosity over the degree of decompression. Following Okumura et al. (2019), two estimates of the magma viscosity were done. The first case

assumes that only the microlites (53 vol.%) oppose the bubble viscous relaxation. The second case assumes that both microlites and alumina (70 vol.%) oppose the bubble viscous relaxation. In both cases, we considered the minimum (negligible expansion) and maximum (deformation rate approximated by the maximum gas volume expansion, 10 vol.%, divided by decompression time) relative viscosity. Figure 2 shows the increase in pressure difference between the bubbles and the medium caused by decompression if the bubbles are unable to grow fast enough to keep pace with the decreasing ambient pressure. Considering our decompression rate, such overpressure is unlikely to have been >1 MPa.

Bubble spherical relaxation, τ_{relax}, is calculated similarly to τ_{ex} but the driving pressure force is the overpressure due to surface tension once the bubble has reached chemical and mechanical equilibrium ($\Delta P = 4\sigma/d$, where $\sigma = 0.07$ N/m is the surface tension and $d = 2l$ is the bubble curvature diameter). This mechanism assumes that capillary forces modified the shape of the bubbles that were not at their equilibrium shape because of the constraining effect of the microlite network. As τ_{relax} depends on the viscosity of the surrounding material, we calculated it for three cases: (a) bubbles are smaller than a microlite, the viscosity considered is that of the melt and bubble mixture (microlite-free and alumina-free, Pal, 2003, $\approx 10^{4-5}$ Pa s); (b) bubbles are larger than a microlite but smaller than a phenocryst, the viscosity considered is that of the melt-bubbles-microlite mixture (Pal, 2003, $\approx 10^{6-7}$ Pa s); (c) for the largest bubbles, the viscosity considered is the melt-microlite-alumina viscosity ($\approx 10^{10-11}$ Pa s). In Case 1, relaxation should occur between 30 s and 5 min, which is on the same order as τ_g. The corresponding small bubbles are thus in a relaxed state at the beginning of the dwelling time. In Case 2, it would take between 40 min and a month to recover a spherical shape. It is thus likely that, during dwelling time, ongoing relaxation causes these medium-sized bubbles to move within the interstitial melt and even move somewhat the microlites. Capillary forces are thus likely to have driven coalescence before this relaxation time is reached, possibly fostering channel formation. This first-order estimate assumes that the curvature relevant to estimate the capillary forces driving the relaxation of these medium-size coalesced bubble chains is at least that of their equivalent spherical diameter. In Case 3, the time to relax a bubble by moving the alumina matrix is $10^{12\sim14}$ s. This estimate is consistent with our observations that no bubble larger than a microlite relaxes into a spherical shape after 1 h 30 min.

The percolation we evidenced differs thus from that starting at higher porosity (Figure S3 in Supporting Information S1), which is proposed to operate relatively high up in the conduit and could be followed by the outgassing of a significant part of the magmatic gases near the sub-surface level. The low porosity thresholds (6–7 vol.% bulk) could be due to an interplay between gravity and surface tension (Parmigiani et al., 2017), or solely due to capillary forces (this study). Percolation in deep parts of volcanic conduits has thus to be considered as a dynamic process even in a stagnant magmatic column.

5. Conclusion: Implication for Volcanic Outgassing

The experimental evidence for primary permeability onset through gas bubble channeling in silicic magmas having at least a bimodal crystal size distribution and gas content lower than 10 bulk vol% has important implications for ascending magmas and eruptive dynamics. We show that the percolation phenomenon is particularly sensitive to the presence of phenocrysts, but less to their sizes. We also see that percolation does not seem to be fostered by a crystalline charge containing only microlites, although this might be due to the unique dwelling time we explored. Even with no deformation, the mechanisms underlying coalescence and the channeling leading to percolation remain dynamic. Therefore, more investigations on the influence of time on percolation process are essential to fully understand permeability at low gas content in deep conduit conditions.

Our permeability values are comparable to those reported in the literature for natural samples (Figure S3 in Supporting Information S1), particularly in dome-forming eruptions like at Merapi, Indonesia (Kushnir et al., 2016). However, it appears that such natural permeabilities correspond to microcracks due to high stress rate occurring relatively high up in the conduit (Shields et al., 2014). This fortuitous match builds on previous works (Heap et al., 2014; Kushnir et al., 2016) that demonstrated the non-unicity of permeability responses because several mechanisms yield similar permeability values. Permeabilities at such low porosity, however, have generally been attributed to microfractures/microcracks (Figure S2B in Supporting Information S1, Kushnir et al., 2016; Shields et al., 2014) that are generally posterior to higher porosity percolation phenomena. In contrast, we attribute the present permeability values to primary percolation (linked to direct coalescence processes) and not to posterior percolation resulting of buoyancy, deformation, or fracturing. It could even imply that the gas channels we observed are preferential sites for subsequent fracturing (Crozier et al., 2022). Here we show that

those permeability values are also consistent with a deep conduit location at rest, that is, coalescence and channeling related percolation.

Our experiments demonstrate the ability of magmas to form permeable channels at low gas content with negligible buoyancy effects (Parmigiani et al., 2017) and without brittle-viscous dynamics (Colombier et al., 2020). This implies that outgassing is possible much deeper in the conduit (Collombet et al., 2021) than previously thought and, in particular, even at the low gas content typical of stagnant magmas (i.e., during repose or inter-eruptive phases, Christopher et al., 2015). Outgassing at such depths requires a high crystallinity composed of at least two populations: phenocrysts inherited from the chamber (Graham et al., 2023; Lindoo et al., 2017) and microlites that typically would have grown in response to the ascent from the chamber into the conduit thanks to the ensuing decompression and a residence time of at least several hours in these new conditions. Efficient outgassing at depth would ultimately delay magma fragmentation as the magma rises to the surface (Gardner et al., 2013; Kendrick et al., 2013; Kushnir et al., 2016). The combination of phenocryst content in the chamber and crystallization conditions near the conduit inlet thus adds an hitherto unrecognized control to the explosive versus effusive behavior of silicic volcanoes in addition to variable speed of ascent through the vent. In this view, phenocrysts act as a primer for outgassing; a necessary but not sufficient condition to gas percolation without magma extrusion. This may be the missing physical mechanism explaining gas transfer across the entire depth of magmatic systems (Collombet et al., 2021; Edmonds et al., 2010; Oppenheimer et al., 2009) despite sometimes very high magma viscosity and low or absent magma extrusion.

Conflict of Interest

The authors declare no conflicts of interest relevant to this study.

Data Availability Statement

Data set for this research are findable and accessible at (Theurel, 2024). It includes full details of the experimental protocol and the complete results of the μ-XCT and SEM analysis.

Acknowledgments
This study is partially supported by the Agence Nationale pour la Recherche MECAMUSH (ANR-19-CE31-0007). This work is part of A. Theurel PhD thesis supported by French national Grant from the Ministère de l'Enseignement Superieur, de la Recherche et de l'Innovation. The computations presented in this paper were performed using the GRICAD infrastructure (gricad.univ-grenoble-alpes.fr), which is supported by Grenoble research communities and μ-XCT devices are supported by the LABEX VOLTAIRE project (ANR-10-LABX-100-01). The authors thank the reviewers and the editor for the constructive comments that helped improve this manuscript.

References

Bretagne, E., Wadsworth, F. B., Vasseur, J., Humphreys, M. C. S., Dingwell, D. B., Dobson, K. J., et al. (2023). The permeability of loose magma mush. *Geology*, *51*(9), 829–832. https://doi.org/10.1130/G51133.1

Burgisser, A., Arbaret, L., Martel, C., Forien, M., & Colombier, M. (2020). The role of oxides in the shallow vesiculation of ascending magmas. *Journal of Volcanology and Geothermal Research*, *406*, 107072. https://doi.org/10.1016/j.jvolgeores.2020.107072

Burgisser, A., Chevalier, L., Gardner, J. E., & Castro, J. M. (2017). The percolation threshold and permeability evolution of ascending magmas. *Earth and Planetary Science Letters*, *470*, 37–47. https://doi.org/10.1016/j.epsl.2017.04.023

Burgisser, A., & Gardner, J. E. (2004). Experimental constraints on degassing and permeability in volcanic conduit flow. *Bulletin of Volcanology*, *67*(1), 42–56. https://doi.org/10.1007/s00445-004-0359-5

Cáceres, F., Scheu, B., Colombier, M., Hess, K.-U., Feisel, Y., Ruthensteiner, B., & Dingwell, D. B. (2022). The roles of microlites and phenocrysts during degassing of silicic magma. *Earth and Planetary Science Letters*, *577*, 117264. https://doi.org/10.1016/j.epsl.2021.117264

Caricchi, L., Burlini, L., Ulmer, P., Gerya, T., Vassalli, M., & Papale, P. (2007). Non-Newtonian rheology of crystal-bearing magmas and implications for magma ascent dynamics. *Earth and Planetary Science Letters*, *264*(3–4), 402–419. https://doi.org/10.1016/j.epsl.2007.09.032

Caricchi, L., Pommier, A., Pistone, M., Castro, J., Burgisser, A., & Perugini, D. (2011). Strain-induced magma degassing: Insights from simple-shear experiments on bubble bearing melts. *Bulletin of Volcanology*, *73*(9), 1245–1257. https://doi.org/10.1007/s00445-011-0471-2

Christopher, T. E., Blundy, J., Cashman, K., Cole, P., Edmonds, M., Smith, P. J., et al. (2015). Crustal-scale degassing due to magma system destabilization and magma-gas decoupling at Soufrière Hills volcano, Montserrat: Degassing at soufrière hills volcano. *Geochemistry, Geophysics, Geosystems*, *16*(9), 2797–2811. https://doi.org/10.1002/2015GC005791

Collombet, M., Burgisser, A., Colombier, M., & Gaunt, E. (2021). Evidence for deep gas loss in open volcanic systems. *Bulletin of Volcanology*, *83*(2), 7. https://doi.org/10.1007/s00445-020-01433-0

Colombier, M., Shea, T., Burgisser, A., Druitt, T. H., Gurioli, L., Müller, D., et al. (2020). Rheological change and degassing during a trachytic Vulcanian eruption at Kilian Volcano, Chaîne des Puys, France. *Bulletin of Volcanology*, *82*(12), 78. https://doi.org/10.1007/s00445-020-01420-5

Crozier, J., Tramontano, S., Forte, P., Oliva, S. J. C., Gonnermann, H. M., Lev, E., et al. (2022). Outgassing through magmatic fractures enables effusive eruption of silicic magma. *Journal of Volcanology and Geothermal Research*, *430*, 107617. https://doi.org/10.1016/j.jvolgeores.2022.107617

Daffos, C., Martel, C., Arbaret, L., & Champallier, R. (2024). Bubble connectivity in experimentally-sheared crystal-bearing silicic melts. *Comptes Rendus Geoscience*, *356*(S1), 1–18. https://doi.org/10.5802/crgeos.214

de Graffenried, R. L., Larsen, J. F., Graham, N. A., & Cashman, K. V. (2019). The influence of phenocrysts on degassing in crystal-bearing magmas with rhyolitic groundmass melts. *Geophysical Research Letters*, *46*(10), 5127–5136. https://doi.org/10.1029/2018GL081822

Degruyter, W., Parmigiani, A., Huber, C., & Bachmann, O. (2019). How do volatiles escape their shallow magmatic hearth? *Philosophical Transactions of the Royal Society A: Mathematical, Physical & Engineering Sciences*, *377*(2139), 20180017. https://doi.org/10.1098/rsta.2018.0017

Drignon, M. J., Bechon, T., Arbaret, L., Burgisser, A., Komorowski, J., Martel, C., et al. (2016). Preexplosive conduit conditions during the 2010 eruption of Merapi volcano (Java, Indonesia). *Geophysical Research Letters*, *43*(22). https://doi.org/10.1002/2016GL071153

Edmonds, M., Aiuppa, A., Humphreys, M., Moretti, R., Giudice, G., Martin, R. S., et al. (2010). Excess volatiles supplied by mingling of mafic magma at an andesite arc volcano: Excess volatiles supplied by underplating. *Geochemistry, Geophysics, Geosystems*, *11*(4). https://doi.org/10.1029/2009GC002781

Forien, M., Arbaret, L., Burgisser, A., & Champallier, R. (2011). Experimental constrains on shear-induced crystal breakage in magmas. *Journal of Geophysical Research*, *116*(B8), B08217. https://doi.org/10.1029/2010JB008026

Gardner, J. E., Ketcham, R. A., & Moore, G. (2013). Surface tension of hydrous silicate melts: Constraints on the impact of melt composition. *Journal of Volcanology and Geothermal Research*, *267*, 68–74. https://doi.org/10.1016/j.jvolgeores.2013.09.007

Giachetti, T., Gonnermann, H. M., Gardner, J. E., Burgisser, A., Hajimirza, S., Earley, T. C., et al. (2019). Bubble coalescence and percolation threshold in expanding rhyolitic magma. *Geochemistry, Geophysics, Geosystems*, *20*(2), 1054–1074. https://doi.org/10.1029/2018GC008006

Gonnermann, H. M., & Manga, M. (2007). The fluid mechanics inside a volcano. *Annual Review of Fluid Mechanics*, *39*(1), 321–356. https://doi.org/10.1146/annurev.fluid.39.050905.110207

Graham, N. A., Larsen, J. F., Tasa, K. Y., deGraffenried, R. L., Cashman, K. V., & McCartney, K. N. (2023). Controls of crystal shape on degassing mechanisms in crystal-rich magmas with rhyolitic groundmass melts. *Earth and Planetary Science Letters*, *601*, 117891. https://doi.org/10.1016/j.epsl.2022.117891

Heap, M. J., Lavallée, Y., Petrakova, L., Baud, P., Reuschlé, T., Varley, N. R., & Dingwell, D. B. (2014). Microstructural controls on the physical and mechanical properties of edifice-forming andesites at Volcán de Colima, Mexico. *Journal of Geophysical Research: Solid Earth*, *119*(4), 2925–2963. https://doi.org/10.1002/2013JB010521

Hess, K.-U., & Dingwell, D. D. (1996). Viscosities of hydrous leucogranitic melts: A non-Arrhenian model. *American Mineralogist*, *81*, 1297–1300.

Jaupart, C., & Allègre, C. J. (1991). Gas content, eruption rate and instabilities of eruption regime in silicic volcanoes. *Earth and Planetary Science Letters*, *102*(3–4), 413–429. https://doi.org/10.1016/0012-821X(91)90032-D

Kendrick, J. E., Lavallée, Y., Hess, K.-U., Heap, M. J., Gaunt, H. E., Meredith, P. G., & Dingwell, D. B. (2013). Tracking the permeable porous network during strain-dependent magmatic flow. *Journal of Volcanology and Geothermal Research*, *260*, 117–126. https://doi.org/10.1016/j.jvolgeores.2013.05.012

Klug, C., & Cashman, K. V. (1996). Permeability development in vesiculating magmas: Implications for fragmentation. *Bulletin of Volcanology*, *58*(2–3), 87–100. https://doi.org/10.1007/s004450050128

Kobayashi, M., Okumura, S., Sasaki, O., & De Silva, S. L. (2023). The role of decompression history in gas bubble formation in crystal-rich silicic magma: Gas retention versus segregation. *Journal of Volcanology and Geothermal Research*, *439*, 107844. https://doi.org/10.1016/j.jvolgeores.2023.107844

Kushnir, A. R. L., Martel, C., Bourdier, J.-L., Heap, M. J., Reuschlé, T., Erdmann, S., et al. (2016). Probing permeability and microstructure: Unravelling the role of a low-permeability dome on the explosivity of Merapi (Indonesia). *Journal of Volcanology and Geothermal Research*, *316*, 56–71. https://doi.org/10.1016/j.jvolgeores.2016.02.012

Laumonier, M., Arbaret, L., Burgisser, A., & Champallier, R. (2011). Porosity redistribution enhanced by strain localization in crystal-rich magmas. *Geology*, *39*(8), 715–718. https://doi.org/10.1130/G31803.1

Lavallée, Y., Miwa, T., Ashworth, J. D., Wallace, P. A., Kendrick, J. E., Coats, R., et al. (2022). Transient conduit permeability controlled by a shift between compactant shear and dilatant rupture at Unzen volcano (Japan). *Solid Earth*, *13*(5), 875–900. https://doi.org/10.5194/se-13-875-2022

Lindoo, A., Larsen, J. F., Cashman, K. V., & Oppenheimer, J. (2017). Crystal controls on permeability development and degassing in basaltic andesite magma. *Geology*, *45*(9), 831–834. https://doi.org/10.1130/G39157.1

Martel, C. (2012). Eruption dynamics inferred from microlite crystallization experiments: Application to Plinian and dome-forming eruptions of Mt. Pelee (Martinique, Lesser Antilles). *Journal of Petrology*, *53*(4), 699–725. https://doi.org/10.1093/petrology/egr076

Mollard, E., Martel, C., & Bourdier, J.-L. (2012). Decompression-induced crystallization in hydrated silica-rich melts: Empirical models of experimental plagioclase nucleation and growth kinetics. *Journal of Petrology*, *53*(8), 1743–1766. https://doi.org/10.1093/petrology/egs031

Morgan, D. J., & Jerram, D. A. (2006). On estimating crystal shape for crystal size distribution analysis. *Journal of Volcanology and Geothermal Research*, *154*(1–2), 1–7. https://doi.org/10.1016/j.jvolgeores.2005.09.016

Mueller, S., Melnik, O., Spieler, O., Scheu, B., & Dingwell, D. B. (2005). Permeability and degassing of dome lavas undergoing rapid decompression: An experimental determination. *Bulletin of Volcanology*, *67*(6), 526–538. https://doi.org/10.1007/s00445-004-0392-4

Okumura, S., De Silva, S. L., Nakamura, M., & Sasaki, O. (2019). Caldera-forming eruptions of mushy magma modulated by feedbacks between ascent rate, gas retention/loss and bubble/crystal framework interaction. *Scientific Reports*, *9*(1), 15845. https://doi.org/10.1038/s41598-019-52272-9

Okumura, S., Nakamura, M., Nakano, T., Uesugi, K., & Tsuchiyama, A. (2012). Experimental constraints on permeable gas transport in crystalline silicic magmas. *Contributions to Mineralogy and Petrology*, *164*(3), 493–504. https://doi.org/10.1007/s00410-012-0750-8

Okumura, S., Nakamura, M., Takeuchi, S., Tsuchiyama, A., Nakano, T., & Uesugi, K. (2009). Magma deformation may induce non-explosive volcanism via degassing through bubble networks. *Earth and Planetary Science Letters*, *281*(3–4), 267–274. https://doi.org/10.1016/j.epsl.2009.02.036

Okumura, S., Nakamura, M., Tsuchiyama, A., Nakano, T., & Uesugi, K. (2008). Evolution of bubble microstructure in sheared rhyolite: Formation of a channel-like bubble network. *Journal of Geophysical Research*, *113*(B7), 2007JB005362. https://doi.org/10.1029/2007JB005362

Oppenheimer, C., Lomakina, A. S., Kyle, P. R., Kingsbury, N. G., & Boichu, M. (2009). Pulsatory magma supply to a phonolite lava lake. *Earth and Planetary Science Letters*, *284*(3–4), 392–398. https://doi.org/10.1016/j.epsl.2009.04.043

Pal, R. (2003). Rheological behavior of bubble-bearing magmas. *Earth and Planetary Science Letters*, *207*(1–4), 165–179. https://doi.org/10.1016/S0012-821X(02)01104-4

Parmigiani, A., Degruyter, W., Leclaire, S., Huber, C., & Bachmann, O. (2017). The mechanics of shallow magma reservoir outgassing. *Geochemistry, Geophysics, Geosystems*, *18*(8), 2887–2905. https://doi.org/10.1002/2017GC006912

Shields, J. K., Mader, H. M., Pistone, M., Caricchi, L., Floess, D., & Putlitz, B. (2014). Strain-induced outgassing of three-phase magmas during simple shear. *Journal of Geophysical Research: Solid Earth*, *119*(9), 6936–6957. https://doi.org/10.1002/2014JB011111

Theurel, A. (2024). Experimental dataset related to "Experimental evidence of primary permeability at very low gas content in crystal-rich silicic magma" by Theurel et al. [Dataset]. *Harvard Dataverse*. https://doi.org/10.7910/DVN/XLTNBG

Vasseur, J., Wadsworth, F. B., Bretagne, E., & Dingwell, D. B. (2022). Universal scaling for the permeability of random packs of overlapping and nonoverlapping particles. *Physical Review E*, *105*(4), L043301. https://doi.org/10.1103/PhysRevE.105.L043301

Wadsworth, F. B., Vasseur, J., Llewellin, E. W., Brown, R. J., Tuffen, H., Gardner, J. E., et al. (2021). A model for permeability evolution during volcanic welding. *Journal of Volcanology and Geothermal Research*, *409*, 107118. https://doi.org/10.1016/j.jvolgeores.2020.107118

References From the Supporting Information

Farquharson, J., Heap, M. J., Varley, N. R., Baud, P., & Reuschlé, T. (2015). Permeability and porosity relationships of edifice-forming andesites: A combined field and laboratory study. *Journal of Volcanology and Geothermal Research*, *297*, 52–68. https://doi.org/10.1016/j.jvolgeores.2015.03.016

Heap, M. J., Troll, V. R., Kushnir, A. R. L., Gilg, H. A., Collinson, A. S. D., Deegan, F. M., et al. (2019). Hydrothermal alteration of andesitic lava domes can lead to explosive volcanic behaviour. *Nature Communications*, *10*(1), 5063. https://doi.org/10.1038/s41467-019-13102-8